Robust estimate of dynamo thresholds in the von Kármán sodium experiment using the Extreme Value Theory

Davide Faranda,, Francois Daviaud, and Bérengère Dubrulle
*Laboratoire SPHYNX, Service de Physique de l'Etat Condensé, DSM, CEA Saclay, CNRS URA 2464, 91191 Gif-sur-Yvette, France**

Mickael Bourgoin,† Sophie Miralles, Philippe Odier, Jean-Francois Pinton, and Nicolas Plihon
Laboratoire de Physique, École Normale Supérieure de Lyon, CNRS & Université de Lyon, 46 allée d'Italie, 69364 Lyon Cedex 07, France

arXiv:1402.4275v1 [physics.flu-dyn] 18 Feb 2014

We apply a new threshold detection method based on the extreme value theory to the von Kármán sodium (VKS) experiment data. The VKS experiment is a successful attempt to get a dynamo magnetic field in a laboratory liquid-metal experiment. We first show that the dynamo threshold is associated to a change of the probability density function of the extreme values of the magnetic field. This method does not require the measurement of response functions from applied external perturbations, and thus provides a simple threshold estimate. We apply our method to different configurations in the VKS experiment showing that it yields a robust indication of the dynamo threshold as well as evidence of hysteretic behaviors. Moreover, for the experimental configurations in which a dynamo transition is not observed, the method provides a way to extrapolate an interval of possible threshold values.

It is generally accepted that the planetary magnetic field is generated by dynamo action, an instability mechanism inside the liquid conducting fluid of the planetary core. There is however presently no general theory providing an estimate for the corresponding dynamo threshold, except in some particular cases [1–3]. The main difficulties in computing the threshold derive from the turbulent nature of the flow, that make the dynamo action akin to a problem of instability in a presence of a multiplicative noise [4]. As more and more data from experiments are available [5–7], the possibility of devising precise, almost automated methods for dynamo threshold detection would be welcome. The statistical approach to this question traditionally involves so-called indicators of criticality [8]. Some of these indicators are based on modifications of the auto-correlation properties of specific observables when parameters controlling the system approach some critical value, others on the fact that an increase of the variance and the skewness is observed when moving towards tipping points [9]. Other approaches are based on the definition of *ad hoc* susceptibility functions or critical exponents [10–12]. In [12, 13], the decay of external applied magnetic field pulses is studied and the transition is detected through the divergence of the decay times near the dynamo threshold. Although interesting for controlled laboratory applications, this approach cannot be extended to problems involving planetary scales. In the present paper, we suggest that the statistical approach based on the Extreme Value Theory proposed in [14] could provide a robust determination of the threshold even in the presence of turbulence. The main advantage of the present method is that it yelds to a precise and unique determination of the threshold as the location of zero crossing of a statistical parameter κ. It therefore works even in the case of imperfect bifurcation that usually occurs in experimental dynamo due to the ambient magnetic field (Earth field, residual magnetization of the disks and other magnetic perturbations of the set up). To illustrate the possibilities of the method, we analyse data from the VKS experiment, consisting of a von Kármán swirling flow of liquid sodium. In this experiment, turbulent effects are roughly of the same order as the mean flow. The control parameter of the system is the magnetic Reynolds number: Rm which is proportional to the driving impellers rotation frequency F. Several dynamo and non dynamo configurations have been obtained by changing the material of the impellers and of the cylinder [12, 15] and by varying the impellers rotation frequency. This versatility allows for reproducing a spectrum of magnetic field dynamics which can be observed for the planetary magnetic fields such as reversal [5], bistability [11, 16] or localization [17]. Applying our method to several different configurations, we show in the present article that it provides a robust indication of the dynamo threshold as well as evidence of hysteretic behaviors.

Method We use the statistical approach based on the Extreme Value Theory proposed in [14] as a criterion allowing the determination of the dynamo threshold. We briefly recall the basic intuition beyond the method referring to [14] for further discussions. Classical Extreme Value Theory (EVT) states that, under general assumptions, the statistics of maxima $M_m = \max\{X_0, X_1, ..., X_{m-1}\}$ of independent and identically distributed (i.i.d.) variables $X_0, X_1, \ldots, X_{m-1}$, with cumulative distribution function (cdf) $F(x)$ in the form:

$$F(x) = P\{a_m(M_m - b_m) \leq x\},$$

where a_m and b_m are normalizing sequences, asymptotically obeys a Generalized Extreme Value (GEV) distribution with cumulative distribution function:

$$F_G(x; \mu, \sigma, \kappa) = \exp\left\{-\left[1 + \kappa\left(\frac{x-\mu}{\sigma}\right)\right]^{-1/\kappa}\right\} \tag{1}$$

with $1 + \kappa(x - \mu)/\sigma > 0$. The *location parameter* $\mu \in \mathbb{R}$ and the *scale parameter* $\sigma > 0$ in Equation 1 account for the normalization of the data, avoiding the recourse to scaling constants a_m and b_m [18].

The sign of κ discriminates the kind of tail decay of the parent distribution: When $\kappa = 0$, the distribution is of Gumbel type (type 1). This is the asymptotic Extreme Value Law (EVL) to be expected when the parent distribution shows an exponentially decaying tail. The Fréchet distribution (type 2), with $\kappa > 0$, is instead observed when the parent distribution possess a fat tail decaying as a power law. Eventually, the Weibull distribution (type 3), with $\kappa < 0$, corresponds to a parent distribution having a finite upper endpoint. When properties of maxima and minima are of interest, respectively corresponding to the exploration of the right or left tails of the parent distribution, they can be treated on an equal footing by considering the minima as maxima of the variables after sign reversal [19]. Physical observables have generally bounded fluctuations and their extremes follow Weibull distributions [20, 21]. Gaussian fluctuations (featuring Brownian motion of microscopic degrees of freedom) would yield the formal possibility of infinite extremes and thus Gumbel distributions, but the convergence towards this law is logarithmically slow [22] so that a Weibull law is observed in these cases as well.

The interest of the EVL statistics in bifurcation detection relies on the change of the nature of the fluctuations of a given system, when going from a situation with one stable attractor to a situation with two competing attractors,

with jump between the two allowed either under the effect of external noise or due to internal chaotic fluctuations. In such a case, two time scale are present, a short one related to transitive dynamics within an attracting component and a long one corresponding to intermittent jumps from one to the other component. The fluctuations and their extreme are then of different nature over the two time scales: over the long time scale, some extremes correspond to noisy excursions directed toward the saddle-state and gain a *global* status as they can trigger jumps from one to the other component. The probability increases as the observable visits corresponding "anomalous" values associated to these global extremes during a time series of length s, and the tail of the parent distribution becomes large. Through the bifurcation, we are thus in a situation where the parent distribution goes from bounded fluctuations (with extreme converging to a Weibull law) to fluctuations with fat tails (with extreme converging to a Fréchet distribution). The shape parameter κ then changes through the bifurcation from $\kappa < 0$ to $\kappa > 0$, wich enables a precise definition of the threshold as the value at which the zero crossing of κ happens. Physical observables will display deviations of greater amplitude in the direction of the state the system is doomed to tumble, than in the opposite direction, therefore one expects to observe this switching either in the maxima or in the minima.

Experimental set-up Here we focus on the VKS experiment, consisting of a von Kármán swirling flow of liquid sodium. The dynamo is generated in a cylinder of radius $R_0 = 289$ mm by the motion of two coaxial discs of radius $R_{imp} = 154.5$ mm, counter-rotating at a frequency F. We define the magnetic Reynolds number as: $Rm = 2\pi\mu_0\sigma R_{imp}R_0F$ where $\sigma = 9.6 \times 10^6\ \Omega\cdot\mathrm{m}^{-1}$ is the sodium electrical conductivity and μ_0 the permeability of vacuum. In the sequel, we use data from the 8 configurations obtained by changing the material of the impellers and of the cylinder as shown in Fig. 2 and described in [12]. Magnetic fields are recorded using four arrays of ten 3-axis Hall effect sensors inserted in radial shafts, as shown in Fig. 1. Two arrays are inserted in the mid-plane of the vessel, within long probe shafts (labeled b and d in Fig. 1); the other two are inserted closer to the impellers, within shorter probe shafts (labeled a and c in Fig. 1). These magnetic field at the sensors are recorded at a rate of 2000 Hz, with accuracy ± 0.1 G. Overall, the probes provide measurements of the 3 components of the magnetc field $\vec{B}(t)$ as a function of time t.

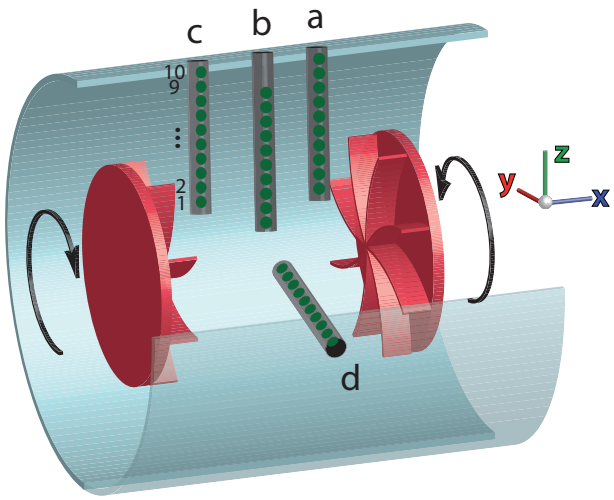

FIG. 1. Experimental setup, showing the location of the Hall probes. x is the axial coordinate directed from impeller 1 to impeller 2

Application to VKS data. We present the results for the detection of the dynamo threshold Rm^* by using as observable the modulus of the magnetic field $|\vec{B}(t)|$ measured by the 40 different detectors (Hall probes).

The method can be described as follows. First of all, the extremes of the magnetic field are extracted by using the so called *block maxima approach* which consists in dividing the series $|\vec{B}(t)|,\ t = 1, 2, ..., s$ into n bins each containing m observations ($s = nm$) and thus selecting the maximum (minimum) M_j in each bin. The series of $M_j, j = 1, ..., n$ is then fitted to the GEV distribution via the L-moment procedure described in [23]. In order to sample proper extreme values one has to consider a bin length longer than the correlation time τ. For each of the sensors we have computed τ as the first zero of the autocorrelation function finding that 0.42 s $< \tau <$ 1 s lags depending on the cases considered. This value is similar to the magnetic diffusion time found in [24]. By choosing a bin duration longer than 1 s (or, equivalently, a number of samples m in each bin larger than 2000) and repeating the fit until the shape

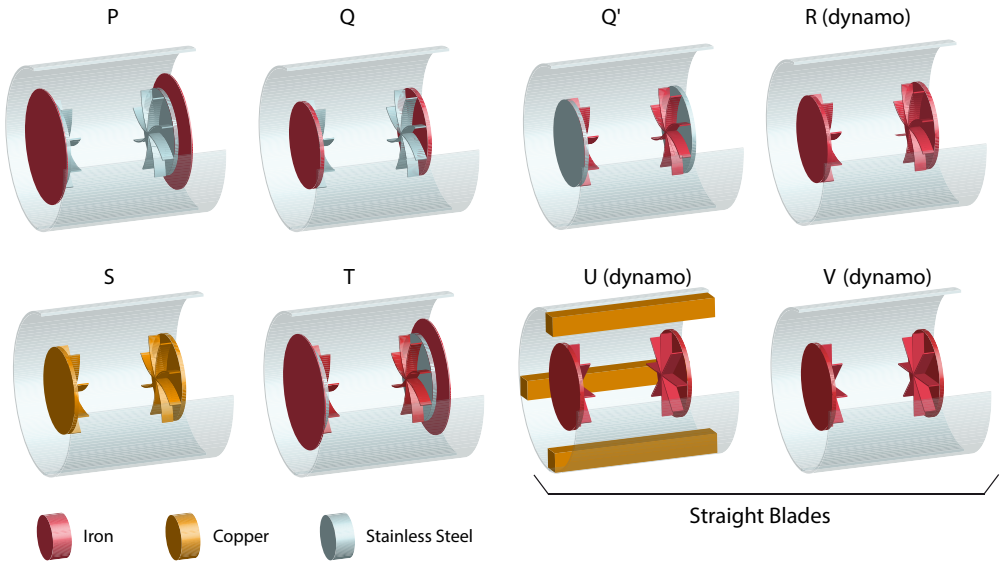

FIG. 2. Schematic representation of the studied VKS configurations. Gray colors stands for stainless steel, yellow color for copper and red for soft iron.

parameter κ is not changing in appreciable way, one can establish the convergence to the GEV model [18]. In our experiments we found that reliable estimates can be generally obtained for $m > 4000$. Being the length of each series $10^5 < s < 3 \cdot 10^5$, for any choice of $m > 4000$ no more than $n = 100$ maxima can be extracted. Such a value of n is one order of magnitude smaller than the one prescribed in [25, 26] for avoiding biased fits to the GEV model. In order to overcome this problem we have grouped sensors located at the same radial position. The sensors of the four arrays of Hall effect sensors are not installed at the same radial distance (see Fig 1 for a visual explanation). However, an effective radial grouping can be obtained by adding to the n extremes of the sensor a_l the ones of b_{l+2}, c_l and d_{l+2}, $l = 1, ..., 8$, thus obtaining 8 different series with a sufficient number of maxima to perform the fit. The choice of grouping the sensors by their radial location is justified by checking that the shape of the distribution, which enters in the computation of the shape parameter κ does not change substantially for sensors located at the same radial position. In order to do so, we have computed the skewness and the kurtosis for the time series of the magnetic field, finding small variations for sensors located at the same radial position. We also checked that the maxima extracted by combining the series are independent by analyzing the cross-correlation function of different sensors. For example, for sensors a and b, the cross-correlation function is defined as:

$$\tilde{\tau}_{M(a),M(b)}(h) = \frac{1}{n}\sum_{i=1}^{n-h}(M_j(a) - \langle M_j(a)\rangle_j)(M_{j+h}(b) - \langle M_j(b)\rangle_j).$$

Here, the notation $\langle\cdot\rangle_j$ indicates the expectation value taken over the j index. The results of this analysis are shown in Fig. 3, for maxima in the case $Rm \simeq 33.8$, sensors index 5, in the R configuration. The plots on the left refer to $m = 1000$, the ones on the right to $m = 4000$. From top to bottom we represent $\tilde{\tau}(h)$ respectively for $h = 0$, $h = +5$ and $h = -5$. The case h=0 corresponds to sensors located at the same radial position, which we grouped in our study. One can observe that although the correlation is non-zero, it is relatively small (about 0.5 for neighboring probes and smaller than 0.2 for non-neighbouring probes), which validates our grouping of the sensors to increase our statistics. In addition, for sensors located at different radial positions the decorrelation is total (see the example at $h = \pm 5$ in figure 3 but the decorrelation already starts at $h = \pm 1$). This indicates that the different series we show are totally independent.

Due to the different size of the fluctuations, extremes have been renormalized using the following, rather standard, definition:

$$\tilde{M}_j(a_l) = \frac{(M_j, a_l - \langle M(a_l)\rangle_j)}{\sqrt{\langle M_j(a_l) - \langle M(a_l)\rangle_j\rangle_j}}$$

The same normalization applies for the sensors b, c, d. There are less trivial ways of normalizing the extremes e.g. by choosing other location indicators than the expected value such as the median or the mode (the most probable

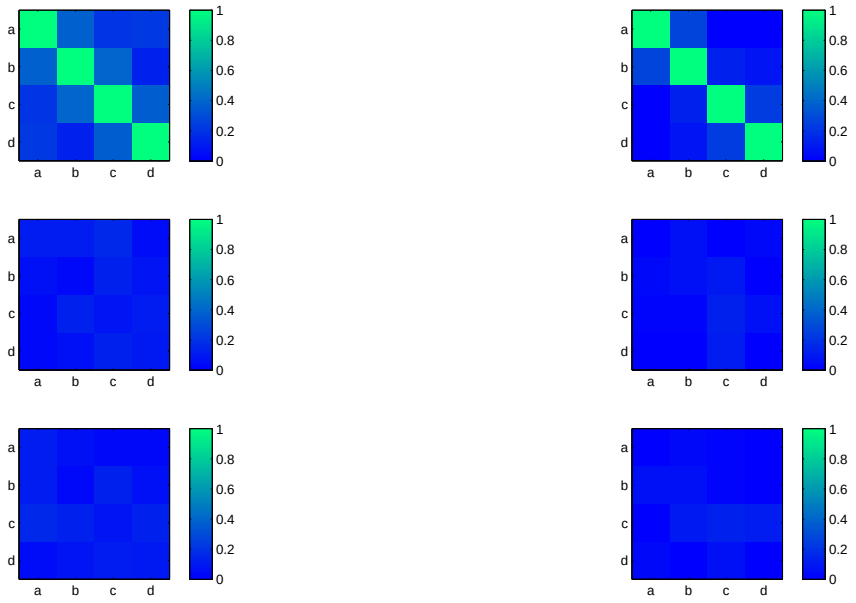

FIG. 3. Cross correlation $\tilde{\tau}_{M(\lambda),M(\mu)}(h)$ for $m = 1000$ (left panels) and $m = 4000$ (right panels) $\lambda = \{a, b, c, d\}$, $\mu = \{a, b, c, d\}$. From top to bottom panels: $h = 0$, $h = 5$, $h = -5$. R configuration, $Rm \simeq 33.8$

value). We thus tested that by replacing the mean with such indicators and checked that the results do not change in an appreciable way.

Results. We begin the analysis by computing dynamo threshold Rm^* in the experiments performed with the configuration R featuring soft iron impellers. This configuration produces a well-documented stationary dynamo at $Rm \approx 44$, thereby providing a fair test of our method [27]. In the run we analyze, the Reynolds magnetic number is increased monotonically from $Rm \simeq 26$ up to $Rm \simeq 54$. By monitoring the value of $|\vec{B}|$ as a function of Rm, represented in the upper panel of Fig. 4, one observes a sudden increase of the magnetic field amplitude around the value $Rm \approx 44$, leading to previous definition of the threshold parameter as $Rm^* = 44$.

The observation of variations of $|\vec{B}|$ provides interesting information about the detection of threshold through EVL method. Indeed, since beyond the dynamo threshold Rm^* the values of $|\vec{B}|$ are significantly higher, we expect to detect the transition by the change of sign of the maxima distribution whereas the minima shape parameter should remain negative even across the transition. Results are shown in Fig. 4 for the shape parameter of the maxima (central panel) and of the minima (lower panel). Each color represents the curve of κ obtained by grouping the sensors located at the same radial position whereas the thick lines respectively represent an average over l (solid black line) and the Gumbel law (dashed black line). When Rm is approaching 47 the average shape parameter for the distribution of maxima first decreases, then increases and changes sign at $Rm = 47$, whereas for the minima it remains negative. We therefore set the threshold value $Rm^* \simeq 47$. The decrease before the change of sign might be a signature of earth-field expulsion before dynamo onset. The change of sign, characteristic of dynamo onset, is associated with a change in the nature of distribution of maxima of the magnetic field, as expected from EVL theory. Indeed, we have plotted in Fig. 5 two histograms for the maxima distribution, one for a value of Rm far from the transition (left plot) and one for Rm close to the bifurcation (right plot). Whereas in the first case the distribution of maxima is bounded above, in the second case the largest values of $\tilde{M}$ will eventually trigger the transition and are responsible for the change of sign of κ. One may note in Fig. 4 that, contrary to the transition presented in [14], here there is an evident effect also on the minima shape parameter which tends to more negative values for $Rm > Rm^*$. This effect, definitely due to the complex geometry of the two attracting basins involved in the transition, is difficult to quantify and will be addressed specifically in future publications.

By analyzing the results obtained at low frequencies of rotations, the fit for each group of sensors returns a shape parameter statistically dispersed around the average, with no radial dependence. On the contrary, for $Rm > Rm^*$ the shape parameter crosses zero for increasing values of Rm as the radial location of the sensors increases. This effect is

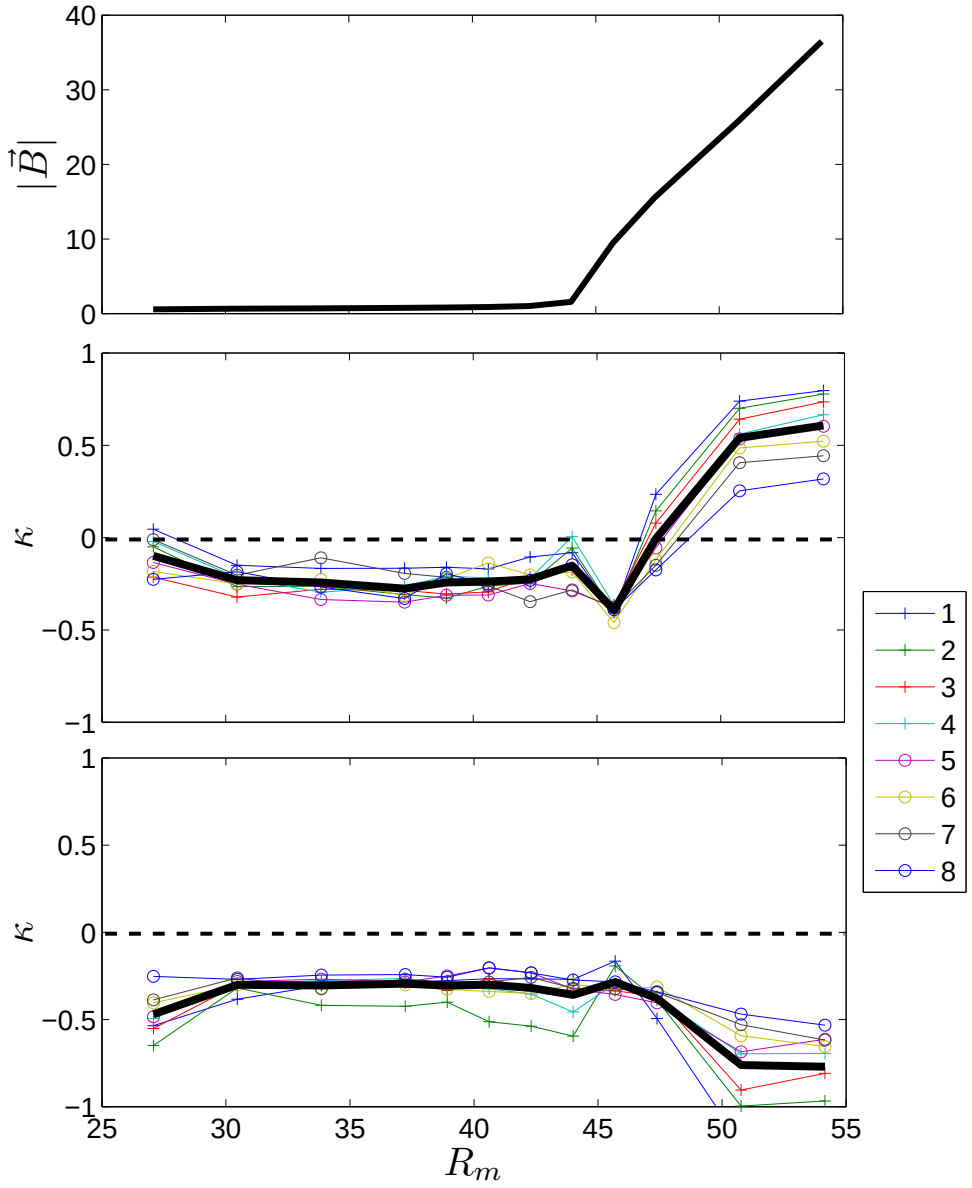

FIG. 4. Upper panel: bifurcation in terms of the magnetic field averaged over all the sensors. Central panel: Shape parameters vs Reynolds magnetic number for the 8 group of sensors (each in a different color), $< k >_l$, (thick black line) and Gumbel law $\kappa = 0$ (dashed line) in the R configuration. Lower panel: same as the central panel but for the minima.

even more pronounced for sensors outside the flow (i;e; sensor 9 and 10 of probes a and c, not shown in Fig. 4 since at these radial locations only two sensors were available instead of 4). This means that the threshold detection based only on external sensors is likely to overestimate the threshold. This has, of course, great implications for the detection of threshold of magnetic fields from planetary observation as we are likely to observe only an equivalent of the outer sensors. This analysis confirms nevertheless a posteriori the reasonableness of grouping the sensors in a radial direction.

Hysteresis has been previously reported in the VKS experiment [10, 27] and was also observed in the R configuration under scrutiny here: in order to shut down the dynamo one has to decrease the magnetic Reynolds number to values smaller than Rm^*. This is presumably an effect of the residual magnetization of the iron impellers. This hysteresis is a good test for further validation of the results obtained via the extreme value based technique since the curve of the shape parameter should be able to detect some hysteretic behavior. If we redefine the dynamo activation threshold

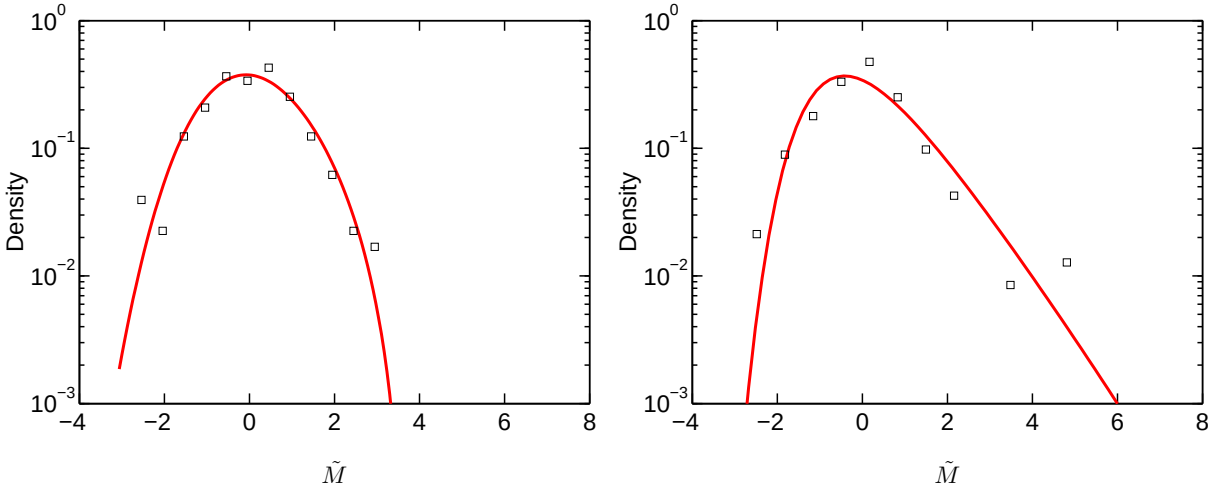

FIG. 5. Two histograms for the normalized maxima $\tilde{M}$ of the sensors 6 (black markers) and correspondent fits to the GEV distribution (red lines). Left: $Rm \simeq 27$ the maxima are bounded: $\kappa = -0.21$. Right: $Rm \simeq 48$, some maxima are detached with respect to the bulk statistics. These events trigger the transition of κ towards positive values: $\kappa = +0.01$.

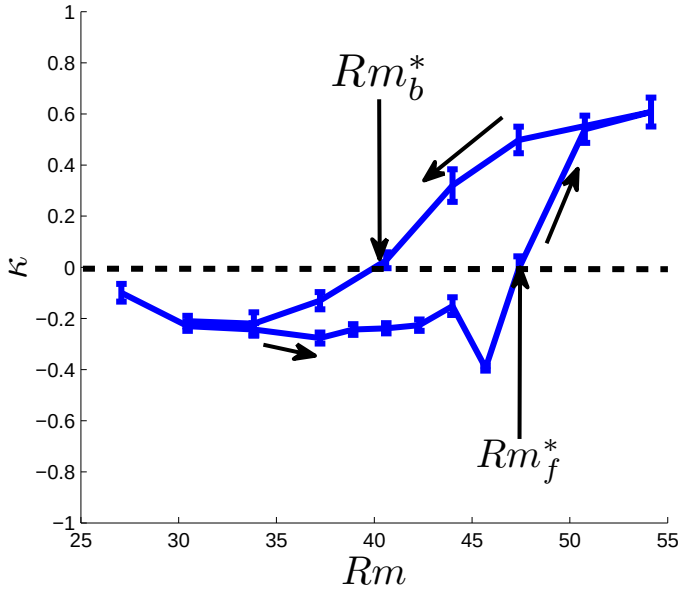

FIG. 6. $\langle\kappa\rangle_l$, (blue line) and Gumbel law $\kappa = 0$ (dashed black line) vs magnetic Reynolds number in the R configuration. The arrows indicate the direction of variation of Rm in the experiment.

found in the previous analysis as $Rm_f^* = 47$, f indicating the first passage in the forward direction of the experiment, we expect to find a dynamo deactivation threshold $Rm_b^* < Rm_f^*$, b indicating the backward experiment obtained by decreasing Rm from $Rm \simeq 55$ to $Rm = 30$. We have then analyzed a run in which the magnetic Reynolds number is first increased monotonically from $Rm \simeq 26$ up to $Rm \simeq 54$, then decreased monotonically from $Rm \simeq 54$ up to $Rm \simeq 26$. The results shown in Fig. 6 for the maxima average shape parameter $\langle\kappa\rangle_l$ $l = 1, ...8$, clearly indicate the presence of a hysteresis cycle in agreement with expectation. We have already commented on the forward part of the experiment repeated in Fig. 6 for clarity and represented by the right arrows. When the frequency is instead decreased, a Fréchet extreme value law is observed until $Rm_b^* \simeq 37 < Rm_f^*$. At this value, the shape parameter crosses the Gumbel law and approaches again the Weibull distribution of the maxima. Note also that the shape parameter for the minima (not shown here) remains always negative even in the backward transition, as expected by the theory described so far.

The same analysis has been carried out for all the configurations shown in Fig. 2. The corresponding Rm_f^* and Rm_b^* are reported in the table below. For comparison, we have included in the table values estimated via three other techniques: from the increase of the magnetic field amplitude $|B|$-denoted $Rm_{|B|}$- [10, 11], from decay time divergence Rm^d[12] and via induction Rm^i [12]. The value of the shape parameter remains negative for both the maxima and the minima, in the configurations P, Q, Q', S, T where dynamos have not been observed, whereas the method is able to detect the dynamo and the hysteretic behavior for the U and V setup. These results are in agreement with [12]. For the configurations for which the dynamo (run P, Q, Q', S, T) is not observed within the range of accessible Rm, it is interesting to follow [12], and try to estimate possible dynamo threshold by extrapolation techniques. Indeed, in the Q', S and T, we observed that the values of κ increase monotonically for at least the 3 consecutive highest Rm. An example is shown for the Q' configuration in Fig. 7. An extrapolate threshold value Rm^e can then be found by applying a polynomial fit of the $\langle\kappa\rangle_l$ curve and detecting the location of the zero crossing. Of course, as seen in Fig. 7, the value of Rm^e depends on the order of the polynomial fit: for example, the value of Rm^e obtained by a linear and a quadratic fit is larger than what is obtained through higher polynomial order fits. We then turned back to configurations R, U, V, and found that a cubic fit of the $\langle\kappa\rangle_l$ values such that $Rm < Rm^*$ provides an extrapolated threshold value Rm^e that is close to the Rm^* determined via real data. We thus run this cubic extrapolation technique to Q', S and T, and obtain value of Rm^e that are reported in the table. The extrapolated values found here are generally smaller than the one found by Miralles et al. [12], but in both cases the extrapolation presents great uncertainty.

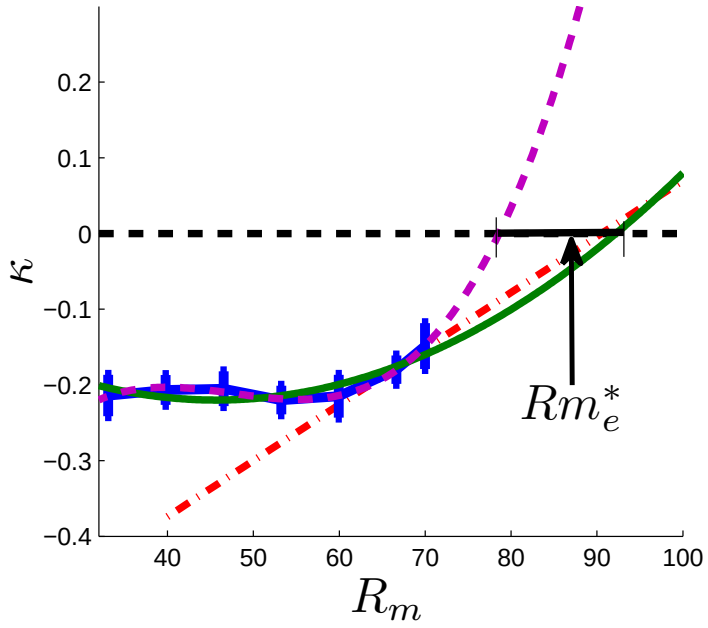

FIG. 7. $\langle\kappa\rangle_l$, (blue solid error-bar) and Gumbel law $\kappa = 0$ (dashed black line) in the Q' configuration vs Reynolds magnetic number. The red dashed-dotted line, the green solid line and the magenta dashed line represent respectively a linear, quadratic and cubic fits of the data. The linear fit is obtained by considering only the 3 values of $\langle\kappa\rangle_l$ at higher Rm. $m = 4000$

In this article, we have tested a methodology for the detection of dynamo threshold based on EVT using datasets produced in the VKS experiment. This technique, applied here for the first time to an experimental dataset, confirms the theoretical expectations of [14] and allows for detecting hysteretic behaviors. The main advantage of the technique is to provide a precise and unambiguous estimate of the thresholds on probabilistic basis, providing the direction of the shift (towards the maxima or the minima). The analysis is affordable with every home PC and many software packages contain the routine necessary for performing the fit of the GEV distribution. In light of the possibility of extracting the magnetic field data from exoplanetary radio emissions, one could exploit the technique described in this article for studying the properties of exo-planetary magneto-spheres thus defining a criterion for the classification of planetary dynamos based on the detected threshold values. Moreover, since hysteretic behaviours are encountered in many other scientific fields, e.g the thermohaline circulation reversibility [28] in climate sciences or the economical crisis behavior [29], we consider the method to be applicable to a more general class of problems featuring critical

Run	$Rm_{\|\|\vec{B}\|}$	Rm_f^*	Rm_b^*	Rm^e	Rm^d	Rm^i
P	-	-	-	-	-	-
Q	-	-	-	-	-	200
Q'	-	-	-	85± 10	350	125
R	44	46	37	-	51	56
S	-	-	-	150± 25	-	-
T	-	-	-	100± 25	250	205
U	70	75	66	-	58	100
V	66	67	45	-	71	93

TABLE I. Dynamo threshold for various configuration in the VKS experiment, obtained through various technique: $Rm_{||\vec{B}|}$: from the increase of the magnetic field amplitude $|\vec{B}|$ [10, 11], Rm_f^* and Rm_b^*: forward and backward threshold obtained from the extreme value technique, with zero crossing detection (this paper); Rm^e: from the extreme value technique, with cubic extrapolation to detect zero crossing (this paper); Rm^d: from decay time divergency extrapolation [12]; Rm^i from induction increase extrapolation.

transitions.

ACKNOWLEDGMENTS

We thank the other members of the VKS collaboration, with whom the experimental runs have been performed. We thank M. Moulin, C. Gasquet, A. Skiara, N. Bonnefoy, D. Courtiade, J.-F. Point, P. Metz, V. Padilla, and M. Tanase for their technical assistance. This work is supported by ANR 08-0039-02, Direction des Sciences de la Matière, and Direction de l'Energie Nucléaire of CEA, Ministère de la Recherche, and CNRS. The experiment is operated at CEA/Cadarache DEN/DTN.

* davide.faranda@cea.fr
† also at Laboratoire des Ecoulements Géophysiques et Industriels, CNRS & Université Joseph Fourier, BP 53, 38041 Grenoble Cedex 9, France

[1] R. Stieglitz and U. Müller, Physics of Fluids **13**, 561 (2001).
[2] K.-H. Rädler, E. Apstein, M. Rheinhardt, and M. Schüler, Studia geophysica et geodaetica **42**, 224 (1998).
[3] A. Gailitis, O. Lielausis, E. Platacis, S. Dement'ev, A. Cifersons, G. Gerbeth, T. Gundrum, F. Stefani, M. Christen, and G. Will, Physical Review Letters **86**, 3024 (2001).
[4] N. Leprovost and B. Dubrulle, The European Physical Journal B-Condensed Matter and Complex Systems **44**, 395 (2005).
[5] M. Berhanu, R. Monchaux, S. Fauve, N. Mordant, F. Pétrélis, A. Chiffaudel, F. Daviaud, B. Dubrulle, L. Marié, F. Ravelet, *et al.*, EPL (Europhysics Letters) **77**, 59001 (2007).
[6] E. Spence, M. Nornberg, C. Jacobson, C. Parada, N. Taylor, R. Kendrick, and C. Forest, Physical review letters **98**, 164503 (2007).
[7] D. H. Kelley, S. A. Triana, D. S. Zimmerman, A. Tilgner, and D. P. Lathrop, Geophysical and Astrophysical Fluid Dynamics **101**, 469 (2007).
[8] M. Scheffer, J. Bascompte, W. A. Brock, V. Brovkin, S. R. Carpenter, V. Dakos, H. Held, E. H. Van Nes, M. Rietkerk, and G. Sugihara, Nature **461**, 53 (2009).
[9] C. Kuehn, Physica D **240**, 1020 (2011).
[10] R. Monchaux, M. Berhanu, S. Aumaître, A. Chiffaudel, F. Daviaud, B. Dubrulle, F. Ravelet, S. Fauve, N. Mordant, F. Pétrélis, *et al.*, Physics of fluids **21**, 035108 (2009).
[11] M. Berhanu, B. Gallet, R. Monchaux, M. Bourgoin, P. Odier, J. Pinton, N. Plihon, R. Volk, S. Fauve, N. Mordant, *et al.*, Journal of Fluid Mechanics **641**, 217 (2009).
[12] S. Miralles, N. Bonnefoy, M. Bourgoin, J.-F. P. Odier, P. Nicolas, G. Verhille, J. Boisson, F. Daviaud, and B. Dubrulle, Physical Review E **88**, 013002 (2013).
[13] J. Lahjomri, P. Capéran, and A. Alemany, Journal of Fluid Mechanics **253**, 421 (1993).
[14] D. Faranda, V. Lucarini, P. Manneville, and J. Wouters, To appear: Chaos, Solitons and Fractals. Arxiv Preprint 1211.0510 (2013).
[15] J. Boisson, S. Aumaitre, N. Bonnefoy, M. Bourgoin, F. Daviaud, B. Dubrulle, P. Odier, J. Pinton, N. Plihon, and G. Verhille, New Journal of Physics **14**, 013044 (2012).
[16] S. e. a. Miralles, Preprint (2014).

[17] B. Gallet, S. Aumaître, J. Boisson, F. Daviaud, B. Dubrulle, N. Bonnefoy, M. Bourgoin, P. Odier, J.-F. Pinton, N. Plihon, *et al.*, Physical Review Letters **108**, 144501 (2012).

[18] M. R. Leadbetter, G. Lindgren, and H. Rootzén, *Extremes and related properties of random sequences and processes*, Springer Series in Statistics (Springer-Verlag, New York, 1983) pp. xii+336.

[19] S. Coles, *An introduction to statistical modeling of extreme values* (Springer Verlag, 2001).

[20] M. P. Holland, R. Vitolo, P. Rabassa, A. E. Sterk, and H. W. Broer, Physica D **241**, 497 (2012).

[21] V. Lucarini, D. Faranda, G. Turchetti, and S. Vaienti, Chaos **22**, 023135 (2012).

[22] P. Hall, Journal of Applied Probability , 433 (1979).

[23] D. Faranda, V. Lucarini, G. Turchetti, and S. Vaienti, to appear in Int. J. of Bifurcat. Chaos (2012).

[24] M. Bourgoin, L. Marié, F. Pétrélis, C. Gasquet, A. Guigon, J.-B. Luciani, M. Moulin, F. Namer, J. Burguete, A. Chiffaudel, *et al.*, Physics of Fluids **14**, 3046 (2002).

[25] J.-P. Eckmann and D. Ruelle, Physica D: Nonlinear Phenomena **56**, 185 (1992).

[26] D. Faranda, V. Lucarini, G. Turchetti, and S. Vaienti, J. Stat. Phys. **145**, 1156 (2011).

[27] M. Berhanu, G. Verhille, J. Boisson, B. Gallet, C. Gissinger, S. Fauve, N. Mordant, F. Pétrélis, M. Bourgoin, P. Odier, *et al.*, The European Physical Journal B **77**, 459 (2010).

[28] S. Rahmstorf, M. Crucifix, A. Ganopolski, H. Goosse, I. Kamenkovich, R. Knutti, G. Lohmann, R. Marsh, L. A. Mysak, Z. Wang, *et al.*, Geophysical Research Letters **32** (2005).

[29] R. Martin, Journal of Economic Geography **12**, 1 (2012).